Supplementary information

Promoting electrocatalytic nitrogen reduction by introducing low-spin sites in ferromagnetic single-atom alloys

*Yiming Ren, Peiyao Bai, Hongguang Wang, Shilin Wei, and Lang Xu**

MOE Key Laboratory of Coal Processing and Efficient Utilization, School of Chemical Engineering and Technology, China University of Mining and Technology, 1 Daxue Road, Xuzhou, Jiangsu, 221116, China

* E-mail address: lang.xu@cumt.edu.cn (L. Xu)

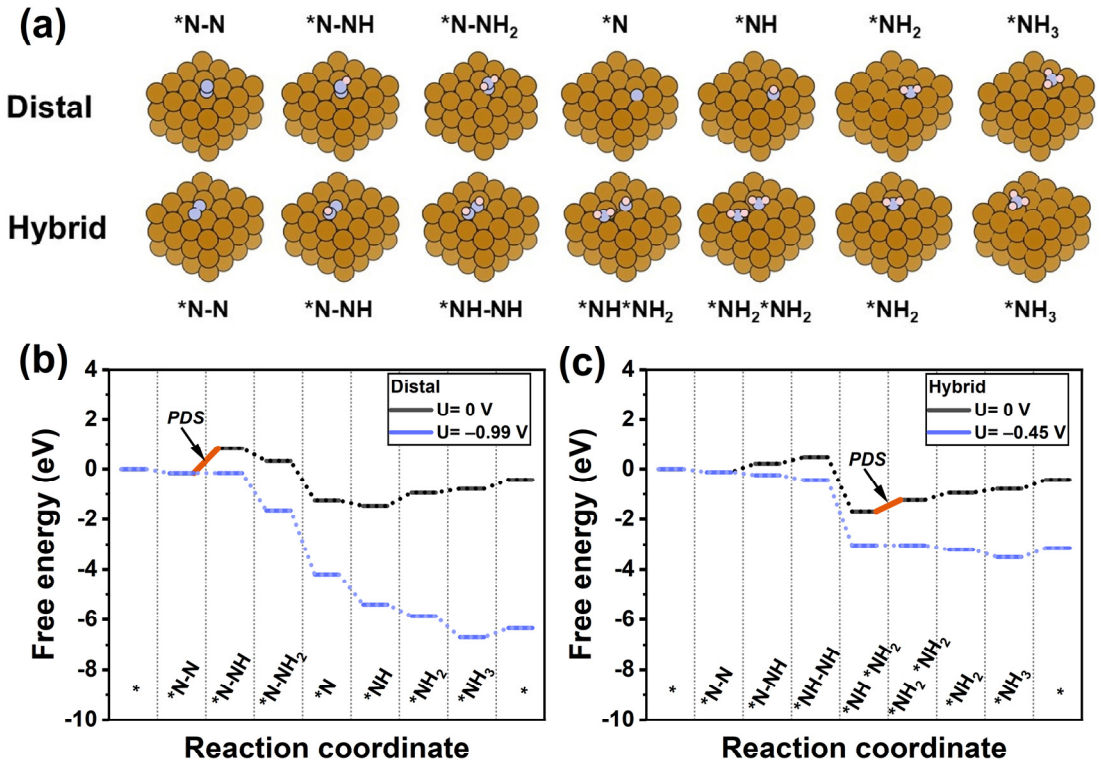

Fig. S1 (a) The electrocatalytic nitrogen reduction reaction (e-NRR) pathways (distal and hybrid) and the intermediate configurations corresponding to the Top and Hollow 1&3 adsorption configurations of N_2. (b) Free energy diagram of the distal pathway. (c) Free energy diagram of the hybrid pathway.

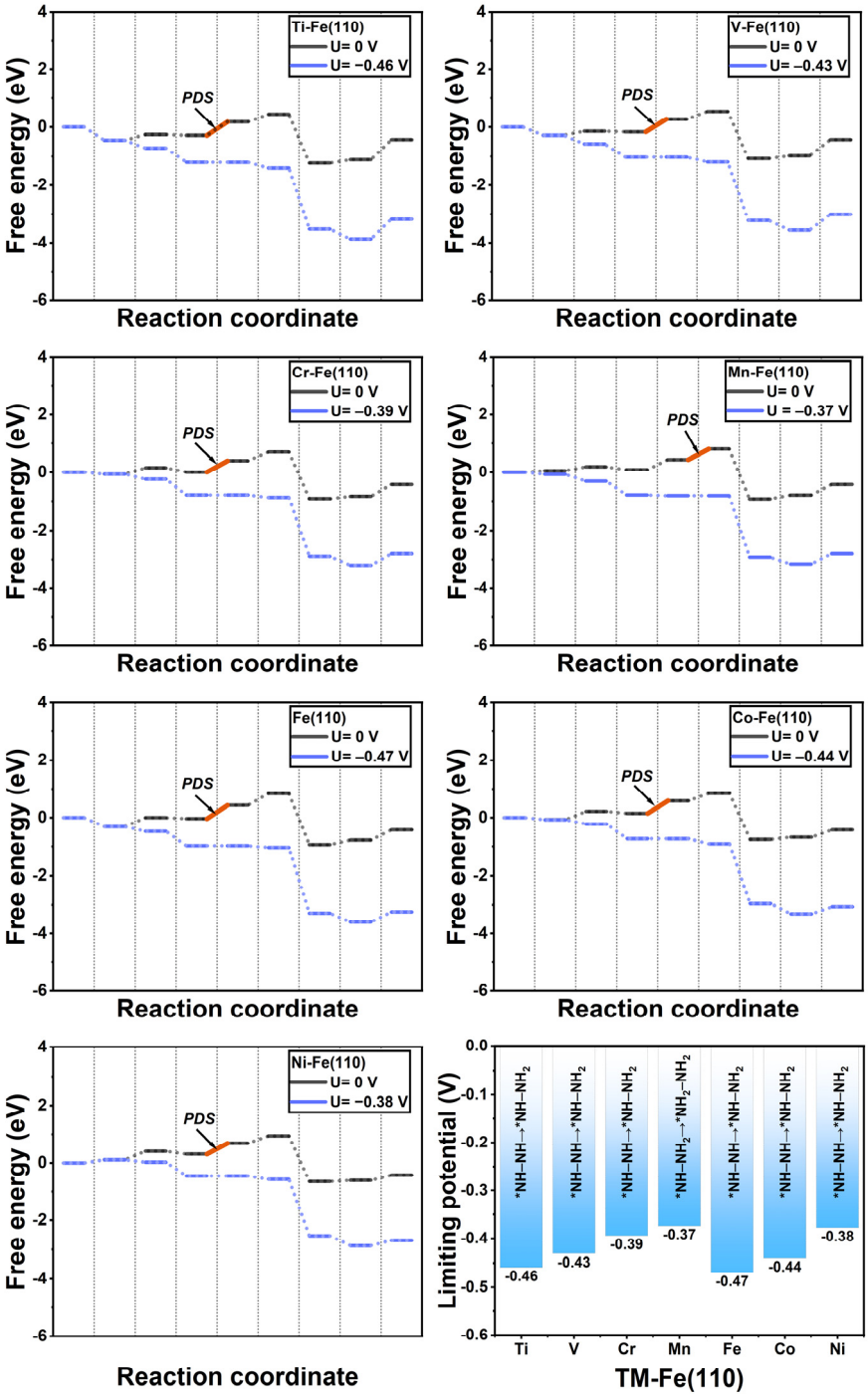

Fig. S2 Free energy diagrams of the intermediates of the fourth-period TM-Fe(110).

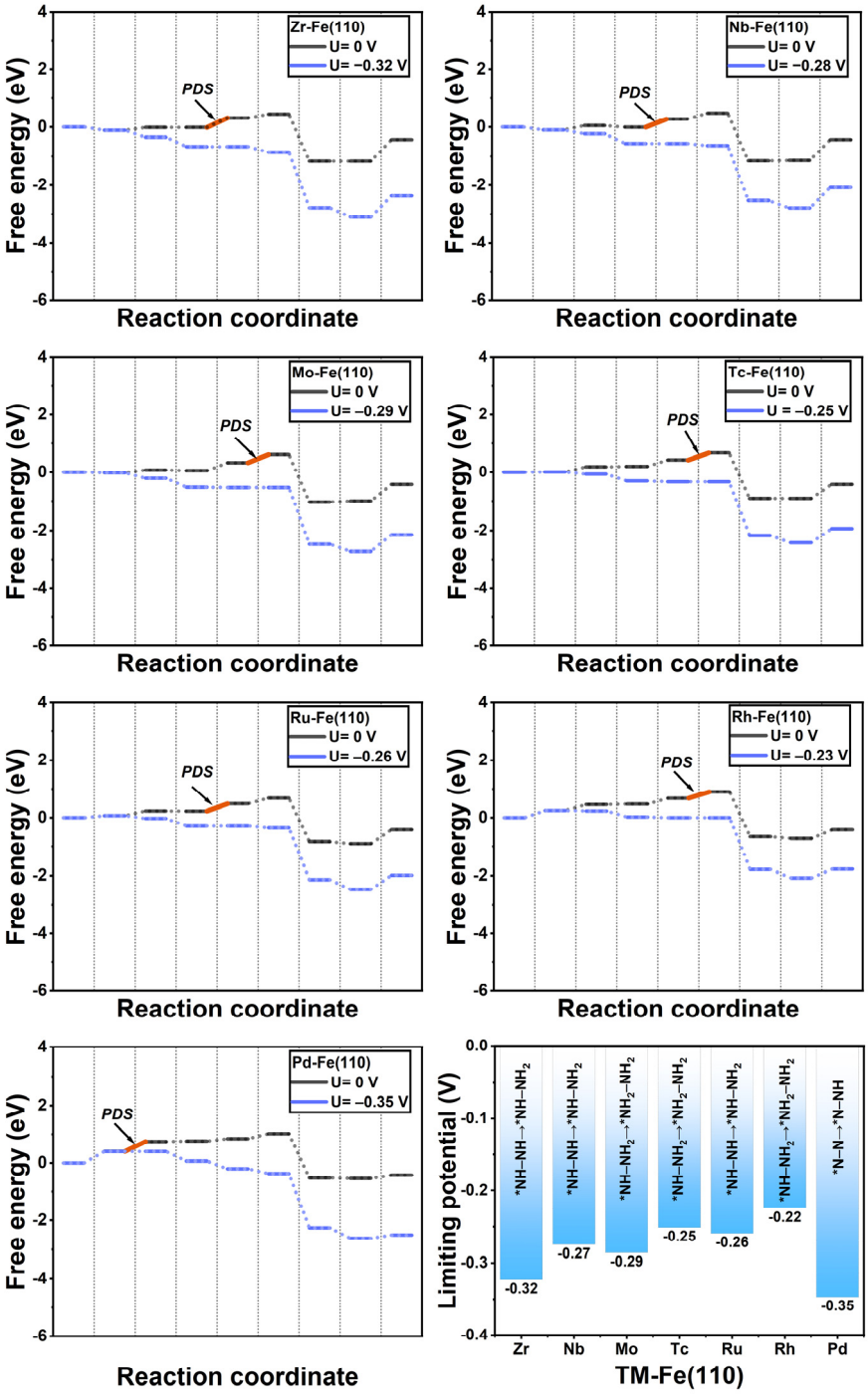

Fig. S3 Free energy diagrams of the intermediates of the fifth-period TM-Fe(110).

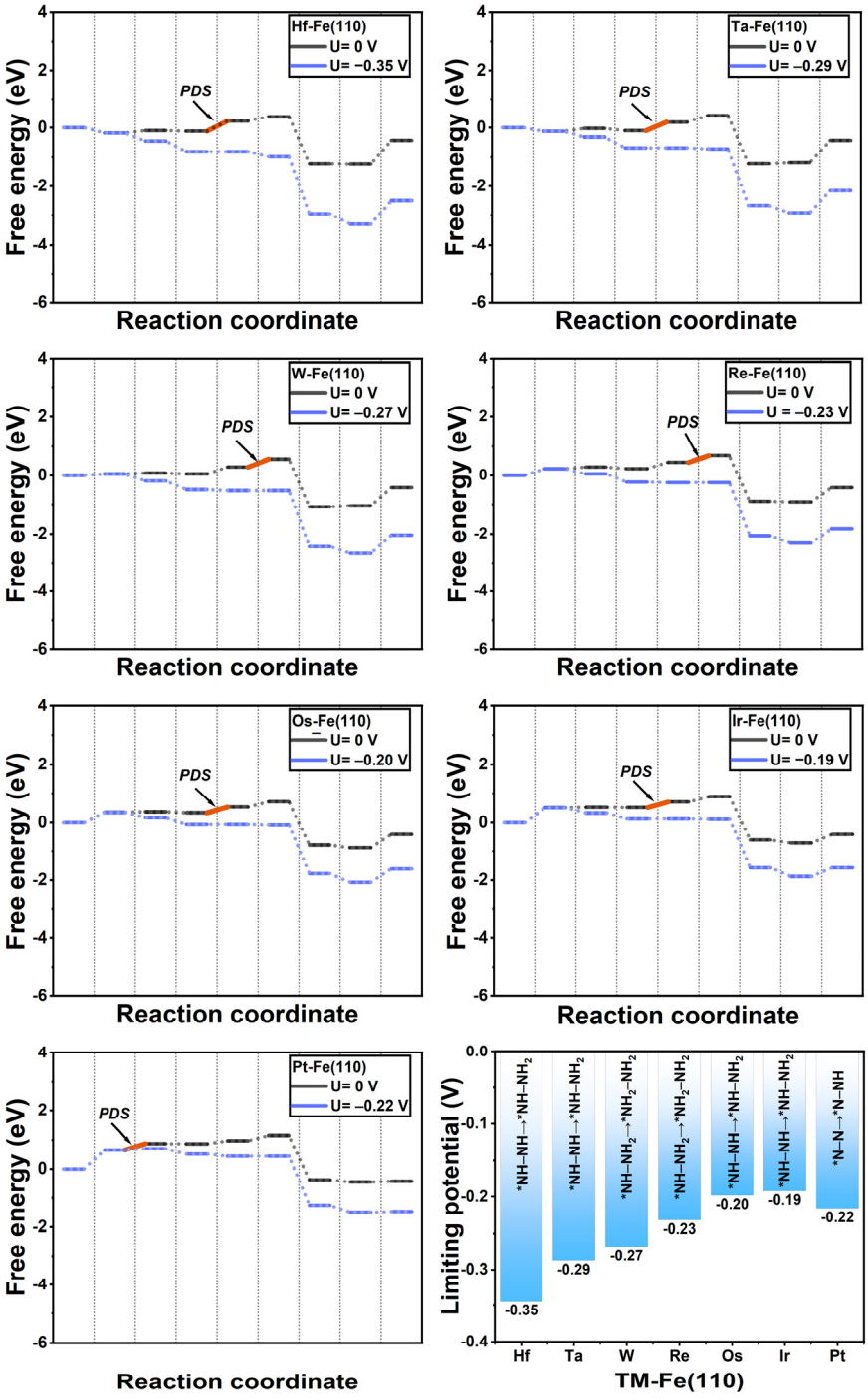

Fig. S4 Free energy diagrams of the intermediates of the sixth-period TM-Fe(110).

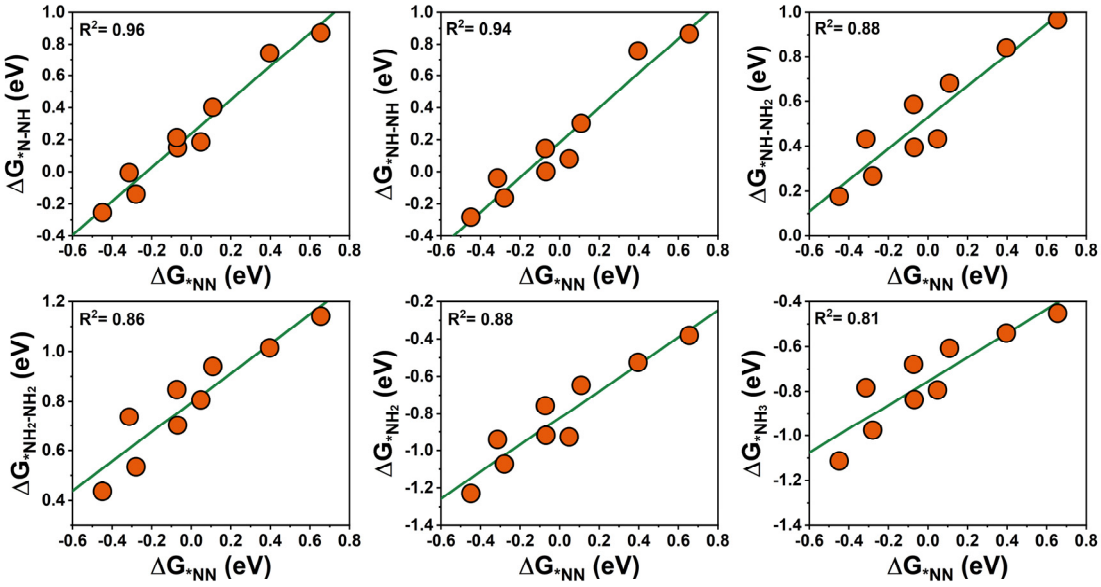

Fig. S5 The scaling relationships between the adsorption Gibbs free energy of the NRR intermediate (ΔG_{*NxHy}) and the N_2 adsorption Gibbs free energy (ΔG_{*NN}) of the fourth-period TM-Fe(110), Pd-Fe(110) and Pt-Fe(110).

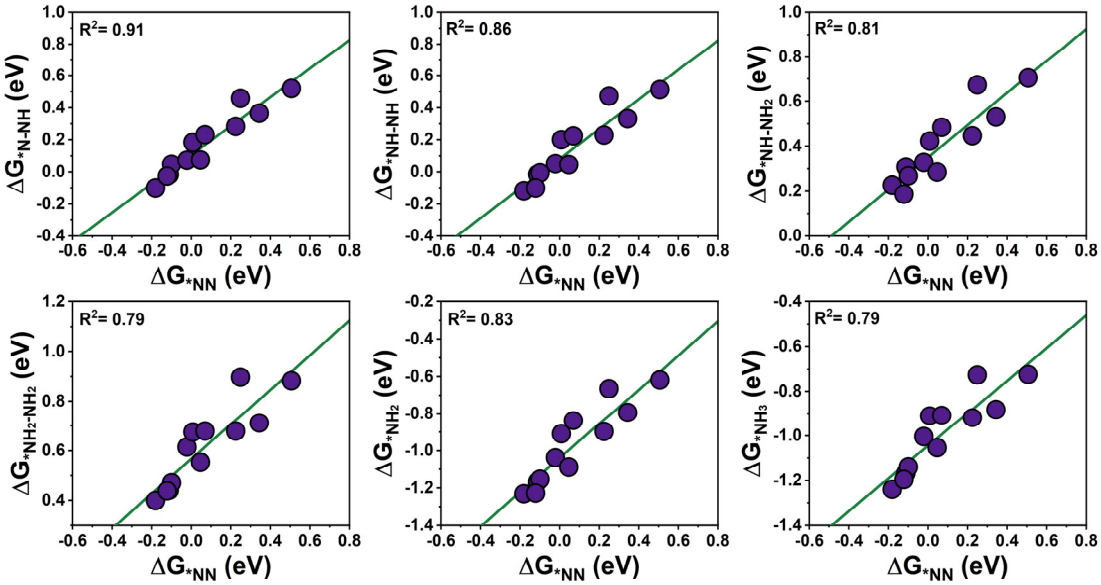

Fig. S6 The scaling relationships between the ΔG_{*NxHy} and ΔG_{*NN} of the fifth- and sixth-period TM-Fe(110), excluding Pd-Fe(110) and Pt-Fe(110).

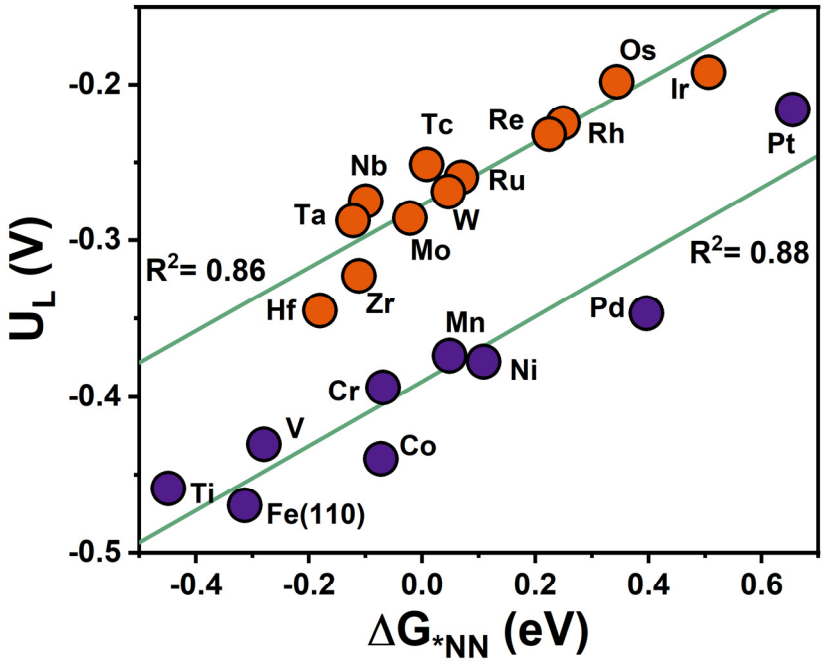

Fig. S7 The scaling relationships between ΔG_{*NN} and the limiting potential of the potential-determining step (U_L) of TM-Fe(110).

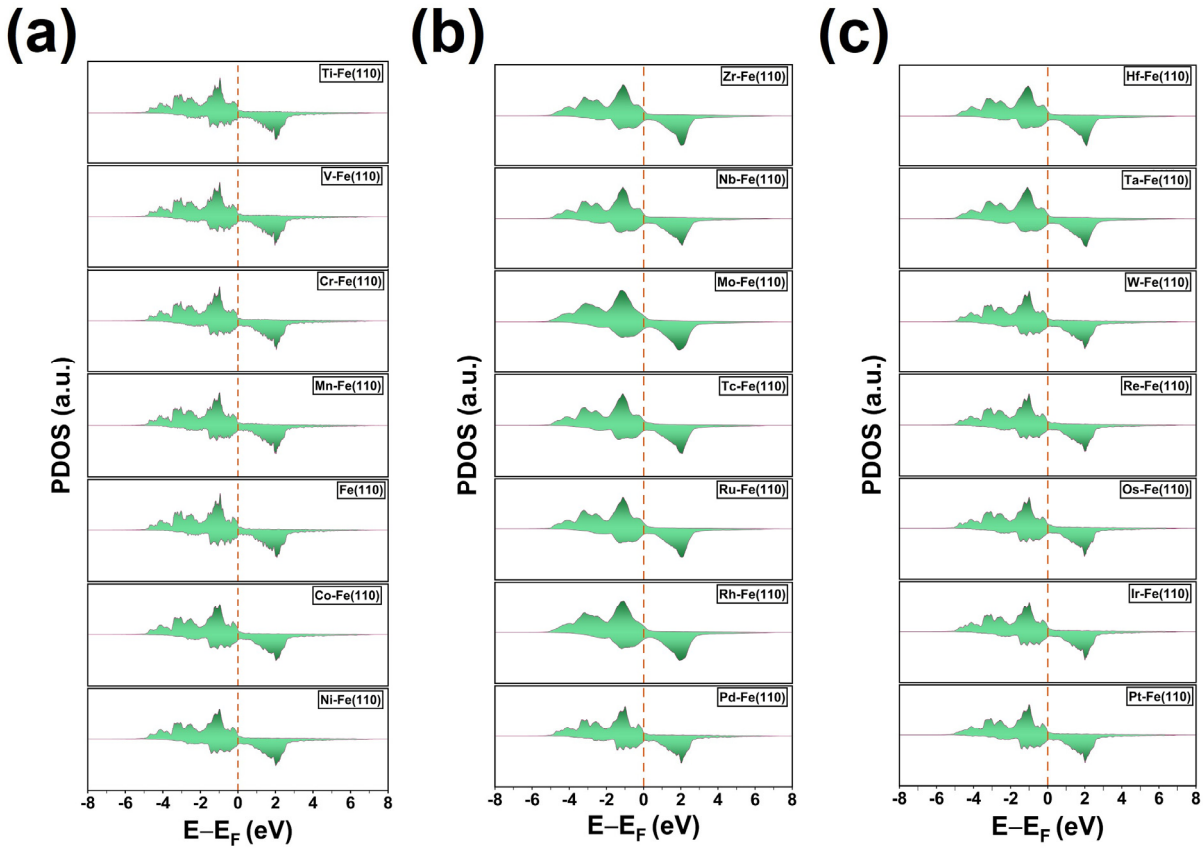

Fig. S8 The d-orbital projected density of states (PDOS) of the fourth-, fifth- and sixth-period TM-Fe(110).

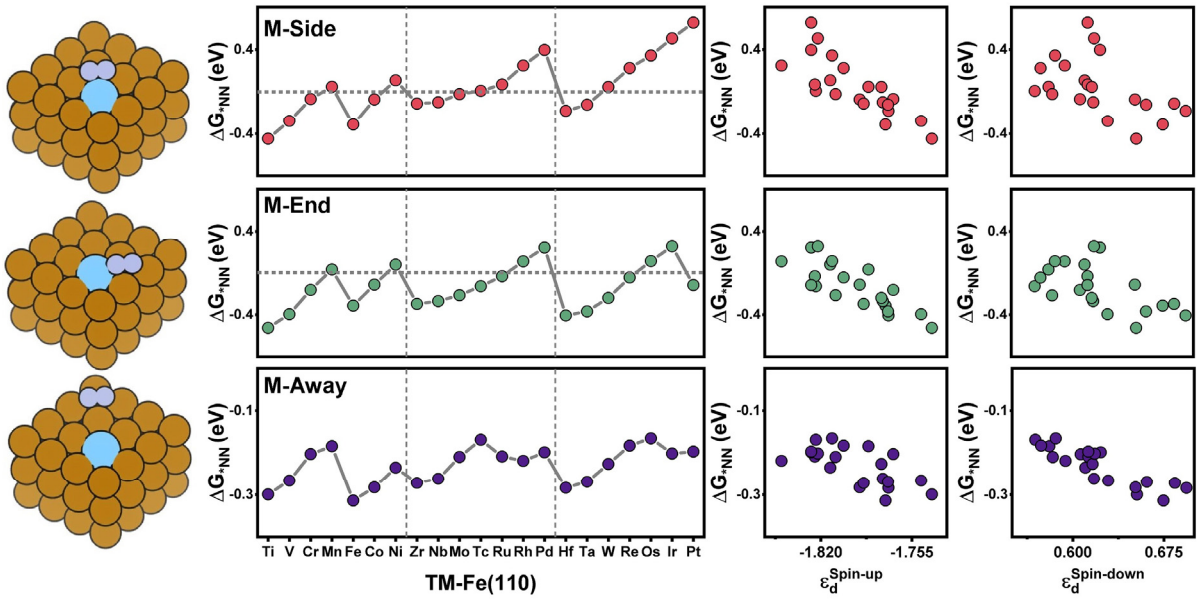

Fig. S9 Three N_2 adsorption configurations (M-Side, M-End and M-Away) and ΔG_{*NN} of the catalysts as well as the relationships between ΔG_{*NN} and spin d-band center of the catalysts (ε_d).

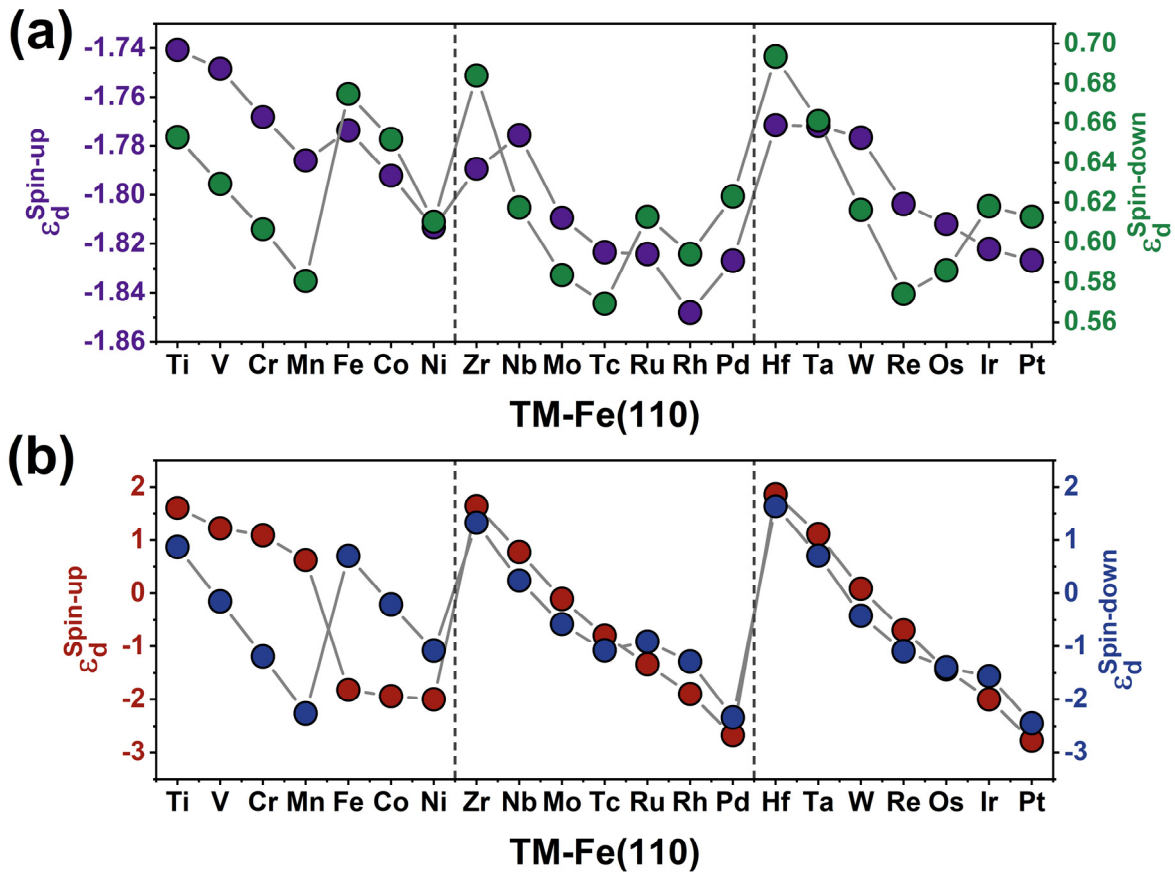

Fig. S10 (a) The values of the spin-up and spin-down d-band centers of TM-Fe(110). (b) The spin-up and spin-down d-band centers of the dopants.

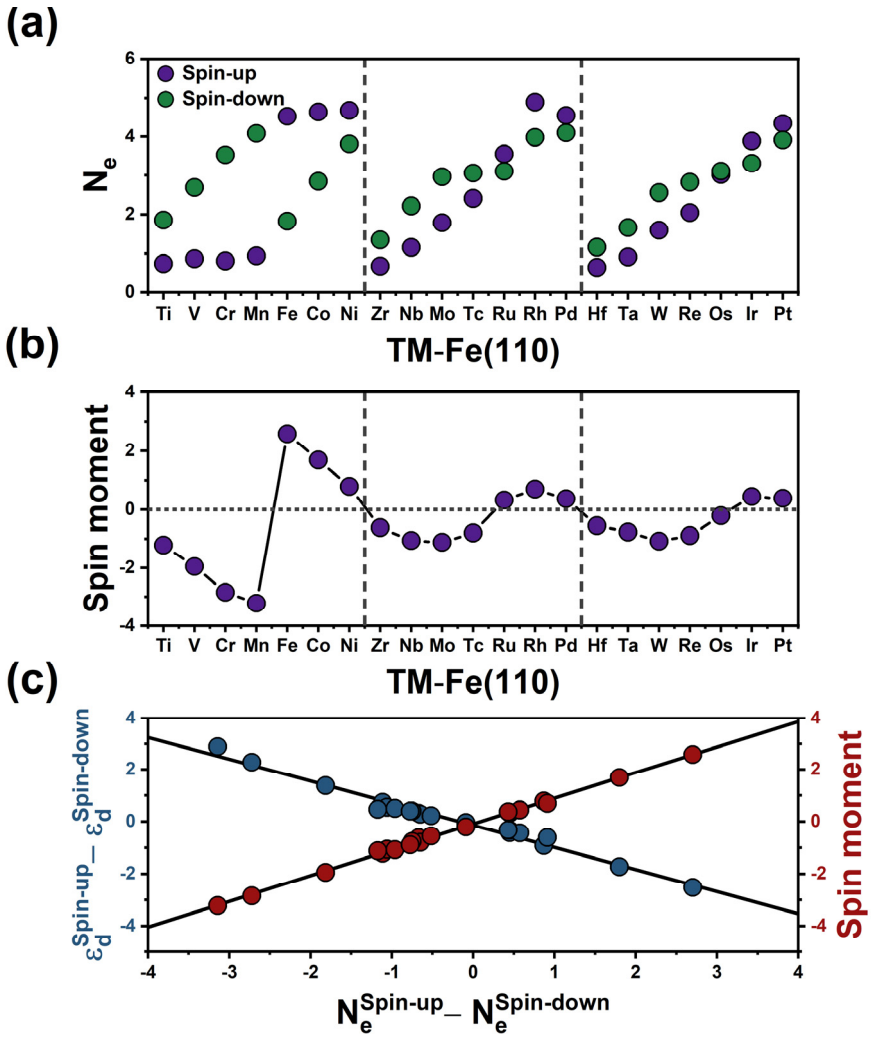

Fig. S11 The electronic structures of the dopants in the TM-Fe(110) catalysts: (a) the number of spin-up and spin-down electrons (N_e), (b) the value of the spin moments, (c) the scaling relationships between the difference in the number of spin d-electrons and the difference in the spin d-band centers and the spin moments.

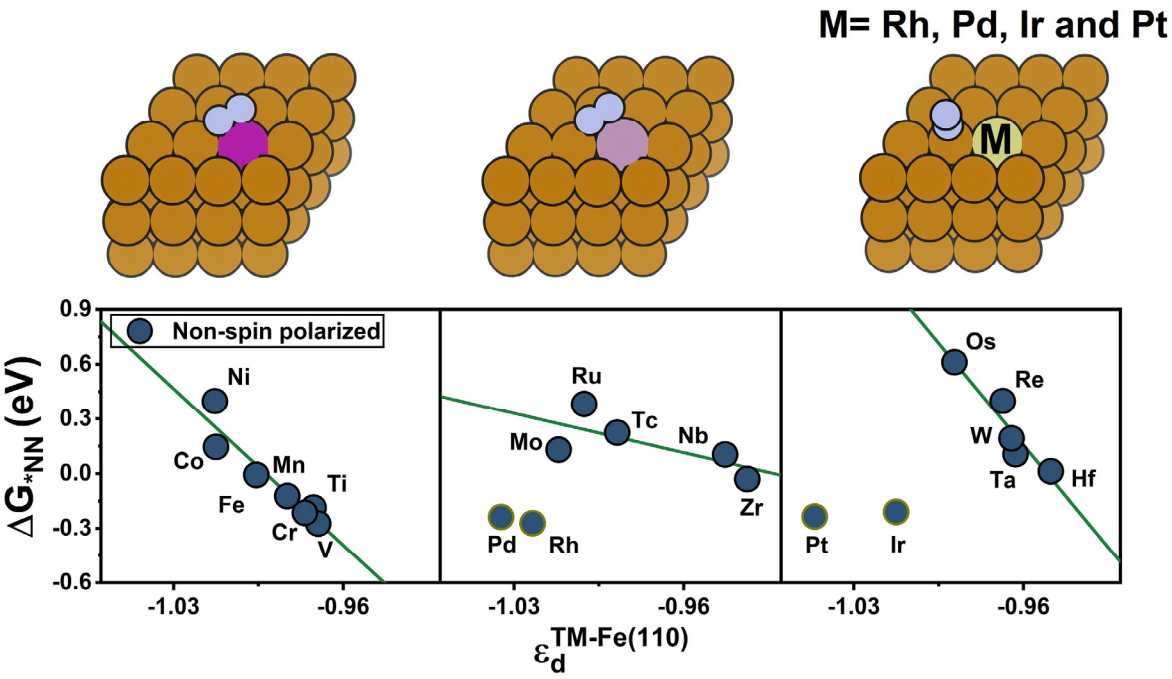

Fig. S12 The scaling relationships between ΔG_{*NN} and the d-band centers of the fourth-, fifth-, and sixth-period catalysts in non-spin polarization calculations.

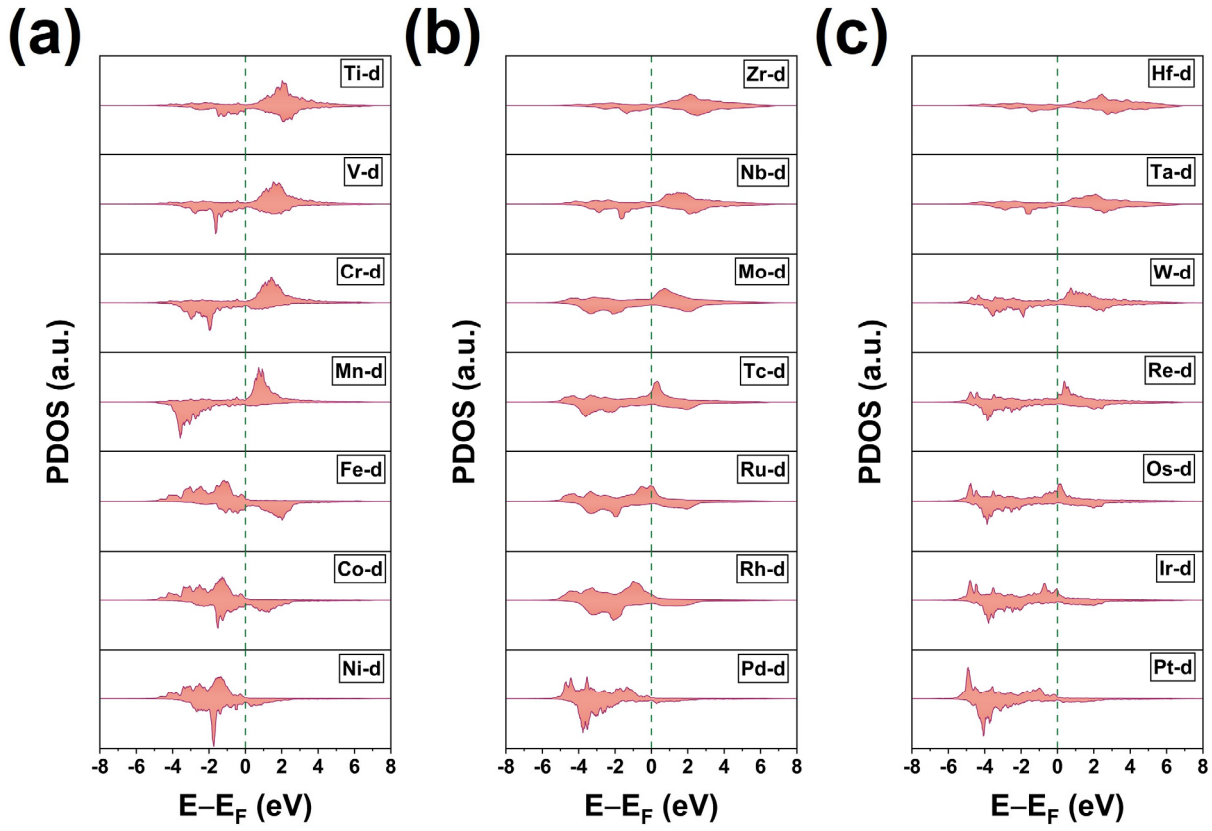

Fig. S13 The d-orbital PDOS of the dopants of the fourth-, fifth-, and sixth-period TM-Fe(110).

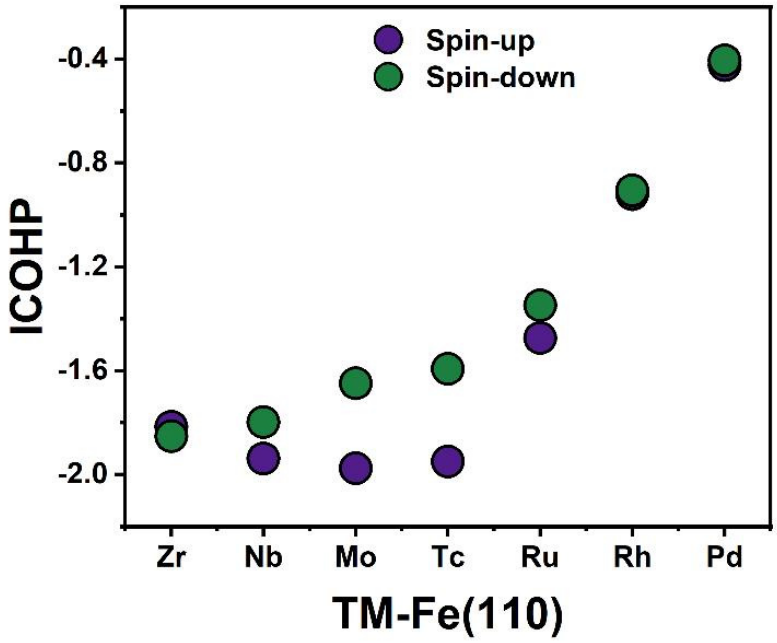

Fig. S14 Integrated projected crystal orbital Hamiltonian population (ICOHP) values of the interaction between the TM sites and N_2 of the fifth-period TM-Fe(110).

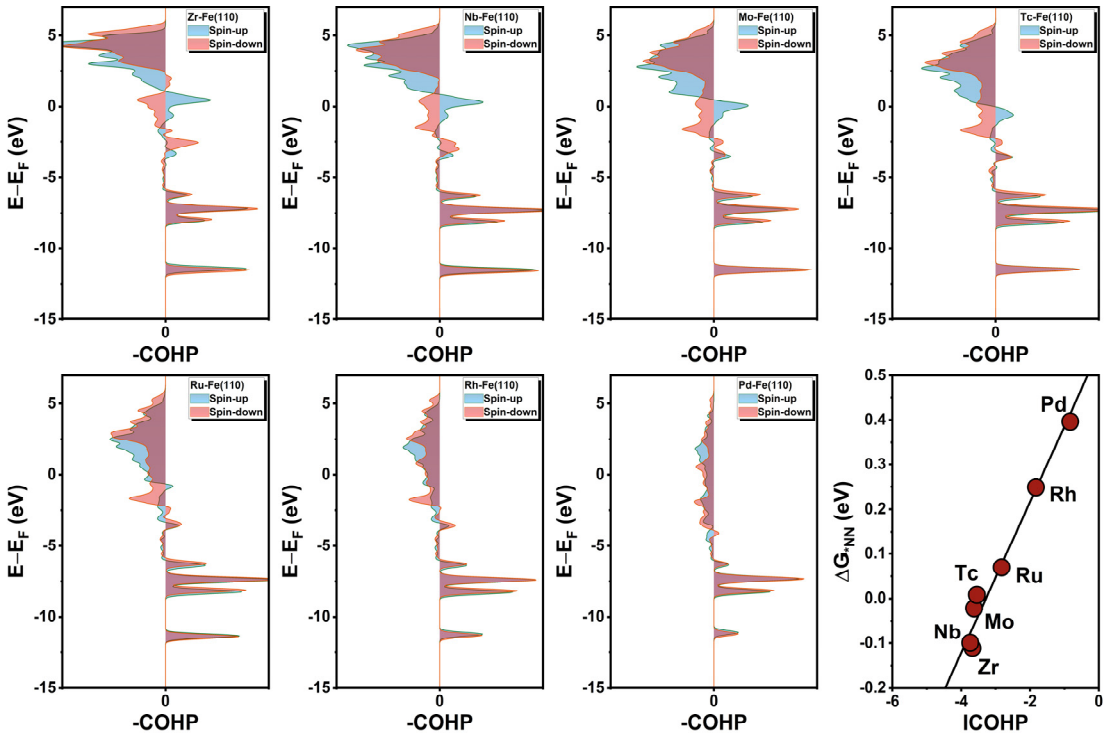

Fig. S15 For the fifth-period TM-Fe(110), the projected crystal orbital Hamiltonian population (COHP) diagrams of the dopants with N_2 as well as the relationship between the ICOHP and ΔG_{*NN}.

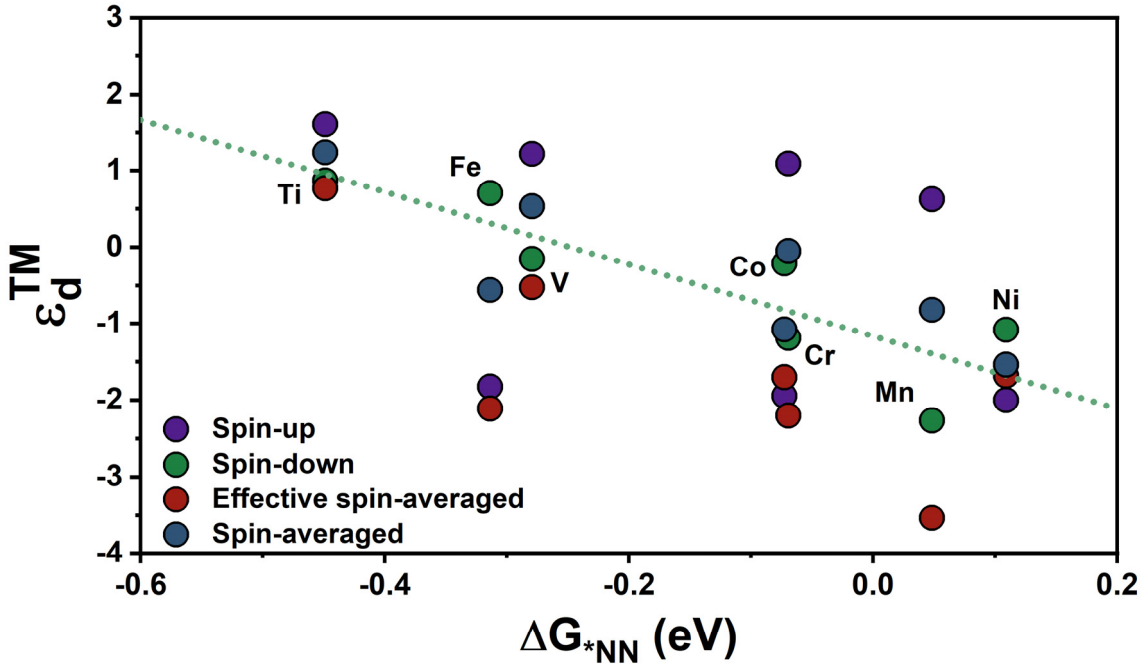

Fig. S16 The relationship between the spin d-band centers of the dopants (ε_d^{TM}) and the ΔG_{*NN} of the fourth-period TM-Fe(110).

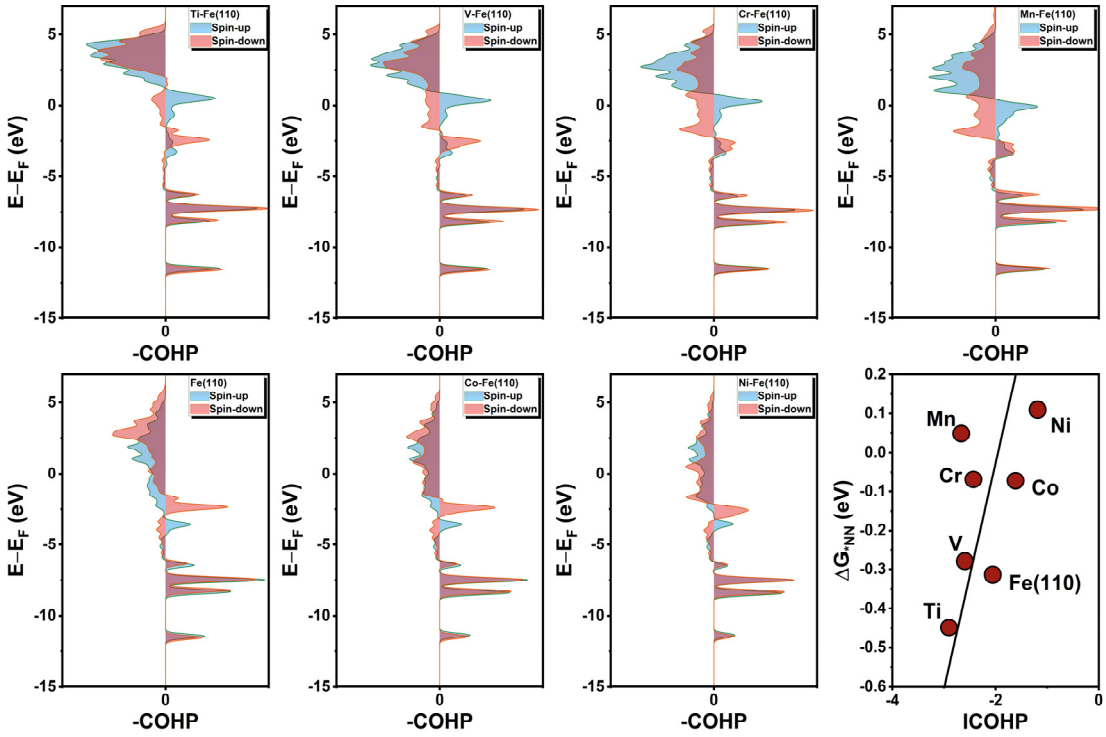

Fig. S17 For the fourth-period TM-Fe(110) catalysts, the projected COHP diagrams of the dopants with N_2 as well as the relationship between the ICOHP and ΔG_{*NN}.

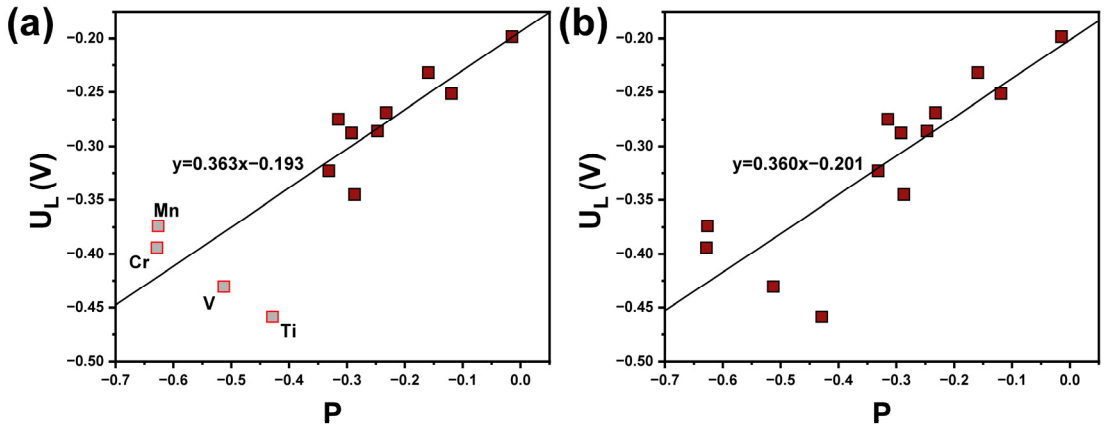

Fig. S18 (a) Excluding Ti, V, Cr and Mn for linear fitting. (b) Including Ti, V, Cr and Mn for linear fitting.

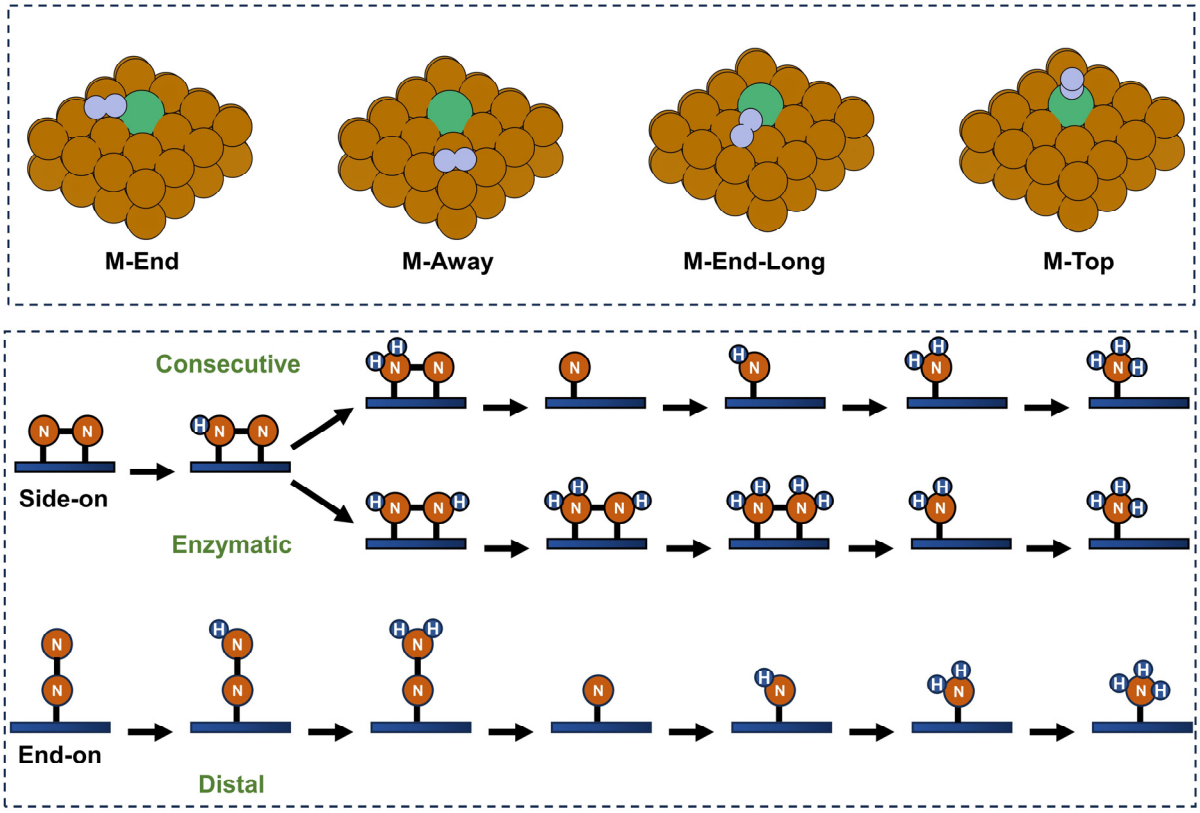

Fig. S19 The four N_2 adsorption configurations on the surfaces of TM-Fe(110) and the reaction pathways corresponding to the side-on and end-on adsorptions.

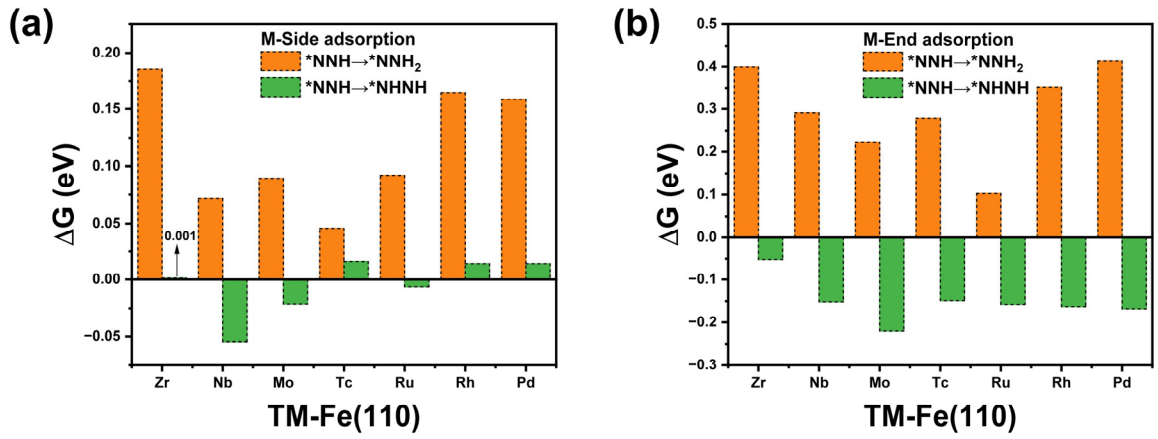

Fig. S20 Gibbs free energy changes (ΔG) for the *NNH→*NNH_2 and *NNH→*NHNH processes. In the e-NRR process with the M-Side and M-End adsorption configurations, the *NNH intermediates tend to form the *NHNH intermediates after the PCET process.

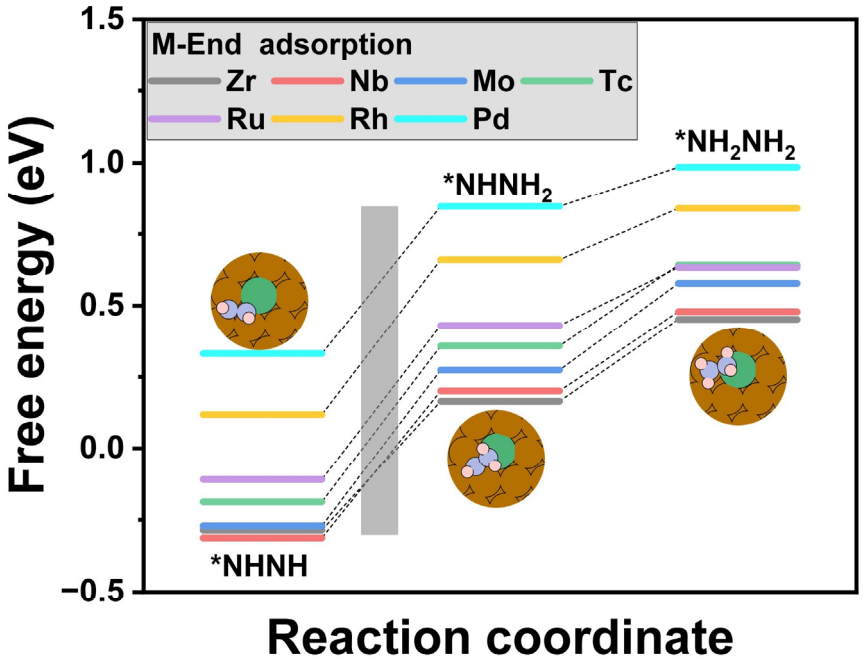

Fig. S21 In the enzymatic pathway corresponding to the M-End adsorption configuration, the *NHNH→*$NHNH_2$ processes have the higher energy barrier than the PDS of the enzymatic pathway corresponding to the M-Side adsorption configuration.

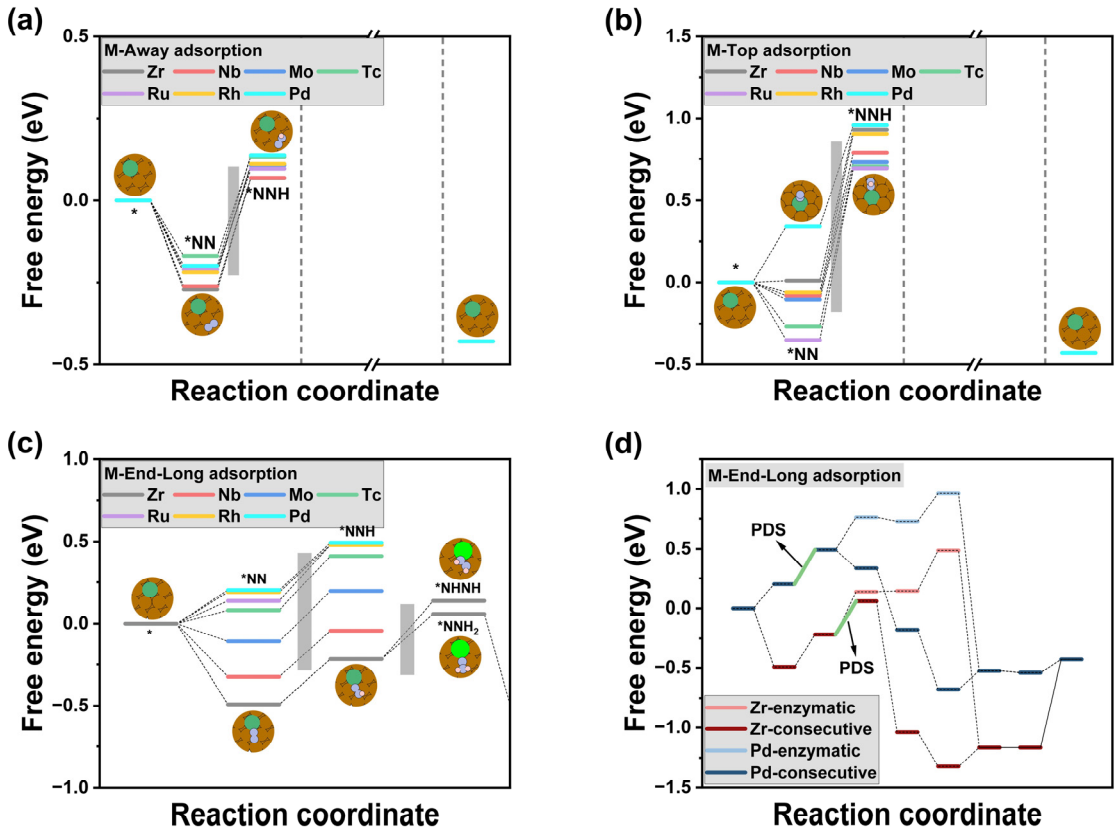

Fig. S22 (a) and (b) In the reaction pathway corresponding to the M-Away and M-Top adsorption configurations, the *NN→*NNH processes have the higher energy barrier than the PDS of the enzymatic pathway corresponding to the M-Side adsorption configuration. Therefore, the DFT energies of the reaction intermediates after the *NNH intermediate are not calculated. (c) and (d) In the reaction pathway corresponding to the M-End-Long adsorption configuration, the *NN→*NNH processes of Pd-Fe(110) and the *NNH→*NNH_2 processes of Zr-Fe(110) have the lower energy barrier than the PDS of the enzymatic pathway corresponding to the M-Side adsorption configuration.

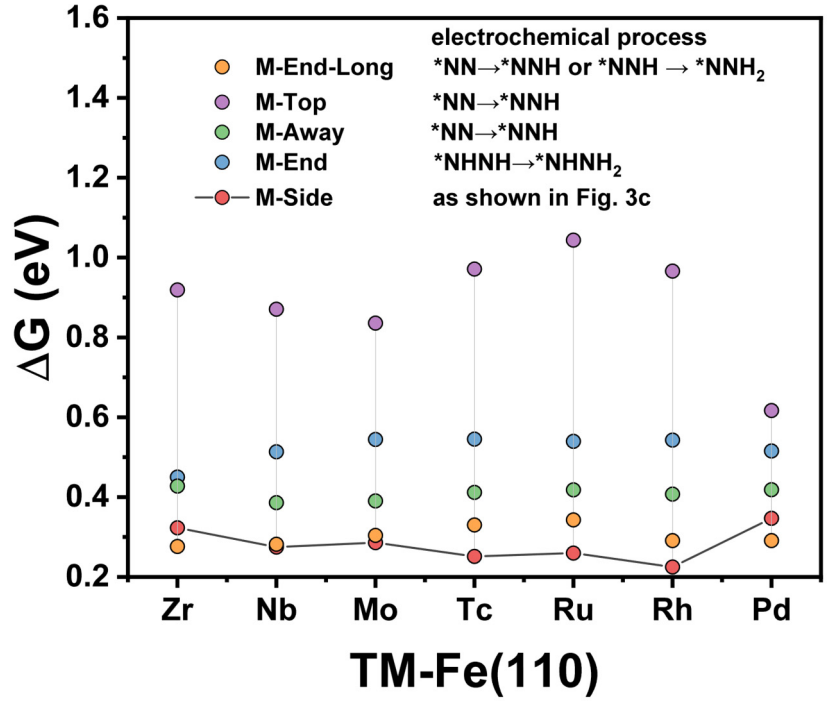

Fig. S23 In the enzymatic pathway corresponding to the M-side adsorption configuration, the ΔG is the energy barrier for the PDS. And in the pathway corresponding to the other four N_2 adsorption conformations, the ΔG is the energy barrier for the given electrochemical process, which is less than or equal to the energy barrier of the PDS.

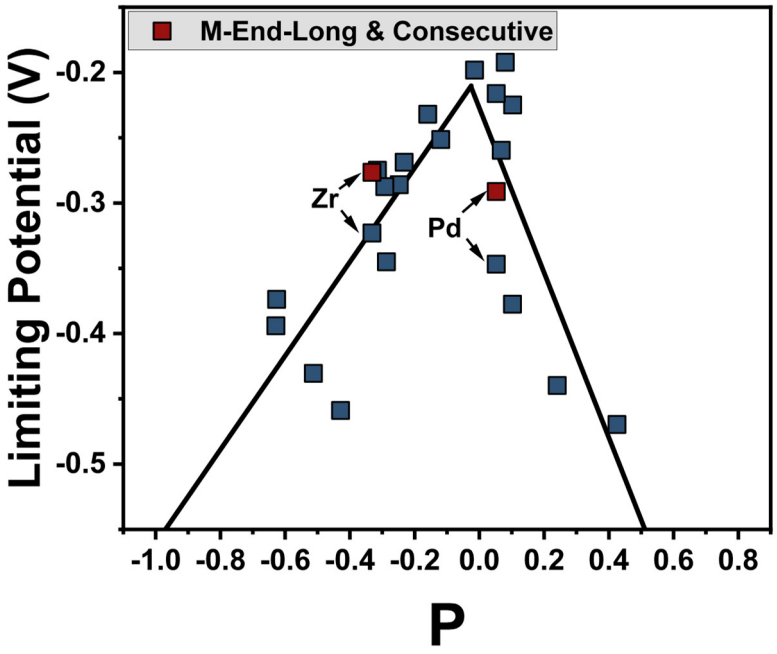

Fig. S24 The limiting potentials of the optimal reaction pathways for Zr-Fe(110) and Pd-Fe(110) remain close to the volcano curve.